Set Functions for Time Series

Anonymous authors
Paper under double-blind review

Abstract

Despite the eminent successes of deep neural networks, many architectures are often hard to transfer to irregularly-sampled and asynchronous time series that occur in many real-world datasets, such as healthcare applications. This paper proposes a novel framework for classifying irregularly sampled time series with unaligned measurements, focusing on high scalability and data efficiency. Our method SEFT (**Se**t **F**unctions for **T**ime Series) is based on recent advances in differentiable set function learning, extremely parallelizable, and scales well to very large datasets and online monitoring scenarios. We extensively compare our method to competitors on multiple healthcare time series datasets and show that it performs competitively whilst significantly reducing runtime.

1 Introduction

With the increasing digitalization, measurements over extensive time periods are becoming ubiquitous. Nevertheless, in many application domains, in particular healthcare (Yadav et al., 2018), measurements might not necessarily be observed at a regular rate or could be misaligned. Moreover, the presence or absence of a measurement and its observation frequency may carry information of its own (Little & Rubin, 2014), such that imputing the missing values is not always desired.

While some algorithms can be readily applied to datasets with varying length, these methods usually assume *regular* sampling of the data and/or require the measurements across modalities to be aligned/synchronized, preventing their application to the aforementioned settings. Existing approaches for *unaligned* measurements, by contrast, typically rely on imputation to obtain a regularly-sampled version of a data set for classification. Learning a suitable imputation scheme, however, requires understanding the underlying dynamics of a system; this task is significantly more complicated and *not* necessarily required when classification is the main goal. Furthermore, even though a decoupled imputation scheme followed by classification is generally more scalable, it may lose information that is relevant for prediction tasks. Approaches that jointly optimize both tasks add a large computational overhead, thus suffering from poor scalability or high memory requirements.

Our method is motivated by the understanding that, while RNNs and similar architectures are well suited for capturing and modelling the dynamics of a time series and thus excel at tasks such as forecasting, retaining the order of an input sequence can even be a disadvantage in classification scenarios (Vinyals et al., 2015). We show that by relaxing the condition that a sequence must be processed in order, we can naturally derive an architecture that *directly* accounts for (i) irregular sampling, and (ii) unsynchronized measurements. Our method SEFT: **Se**t **F**unctions for **T**ime Series, extends recent advances in set function learning to irregular sampled time series classification tasks, yields state-of-the-art performance, is highly scalable and improves over current approaches by almost an order of magnitude in terms of runtime.

With SEFT, we propose to rephrase the problem of classifying time series as classifying a set of observations. We show how *set functions* can be exploited to learn classifiers that are naturally applicable to unaligned and irregularly sampled time series, leading to state-of-the-art performance in irregularly-sampled time series classification tasks. More precisely, SEFT can classify irregular and unaligned time series in time linear in the number of observations m, as compared to the $\mathcal{O}(m \log m)$ runtime of competitor methods that rely on imputation strategies (Li & Marlin, 2016). Furthermore, our approach is highly parallelizable and can be readily extended to an online monitoring setup with up to thousands of patients.

2 RELATED WORK

This paper focuses on classifying time series with irregular sampling and potentially unaligned measurements. We briefly discuss recent work in this field; all approaches can be broadly grouped into the following three categories.

Irregular sampling as missing data While the problem of supervised classification in the presence of missing data is closely related to irregular sampling on time series, there are some core differences. Missing data is usually defined with respect to a number of features that could be observed, whereas time series themselves can have different lengths and a "typical" number of observed values might not exist. Generally, an irregularly-sampled time series can be converted into a missing data problem by discretizing the time axis into non-overlapping intervals, and declaring intervals in which no data was sampled as missing. This approach is followed by Marlin et al. (2012), where a Gaussian Mixture Model was used to do semi-supervised clustering on electronic health records. Similarly, Lipton et al. (2016) discretize the time series into intervals, aggregate multiple measurements within an interval, and add missingness indicators to the input of a Recurrent Neural Network. By contrast, Che et al. (2018) present several variants of the Gated Recurrent Unit (GRU) combined with imputation schemes. Most prominently, the GRU-model was extended to include a decay term (GRU-D), such that the last observed value is decayed to the empirical mean of the time series via a learnable decay term. While these approaches are applicable to irregularly-sampled data, they either rely on imputation schemes or empirical global estimates on the data distribution (our method, by contrast, requires neither), without directly exploiting the global structure of the time series.

Frameworks supporting irregular sampling Some frameworks support missing data. For example, Lu et al. (2008) directly defined a kernel on irregularly-sampled time series, permitting subsequent classification and regression with kernel-based classifiers or regression schemes. Furthermore, Gaussian Processes (Williams & Rasmussen, 2006) constitute a common probabilistic model for time series; they directly permit modelling of continuous time data using mean and covariance functions. Along these lines, Li & Marlin (2015) derived a kernel on Gaussian Process Posteriors, allowing the comparison and classification of irregularly-sampled time series using kernel-based classifiers. Nevertheless, all of these approaches still rely on separate tuning/training of the imputation method and the classifier so that structures supporting the classification could be potentially missed in the imputation step.

End-to-end learning of imputation schemes The following methods are composed of two modules with separate responsibilities, namely an imputation scheme and a classifier, where both components are trained discriminatively and end-to-end using gradient-based training. Recently, Li & Marlin (2016) proposed the Gaussian Process Adapters (GP Adapters) framework, where the parameters of a Gaussian Process Kernel are trained alongside a classifier. The Gaussian Process gives rise to a fixed-size representation of the irregularly-sampled time series, making it possible to apply *any* differentiable classification architecture. This approach was further extended to multivariate time series by Futoma et al. (2017) using Multi-task Gaussian Processes (MGPs) (Bonilla et al., 2008), which allow correlations between the imputed channels. Moreover, Futoma et al. (2017) made the approach more compatible with time series of different lengths by applying a Long Short Term Memory (LSTM) (Hochreiter & Schmidhuber, 1997) classifier. Motivated by the limited scalability of approaches based on GP Adapters, Shukla & Marlin (2019) suggest an alternative imputation scheme, the *interpolation prediction networks*. It applies multiple semi-parametric interpolation schemes to obtain a regularly-sampled time series representation. The parameters of the interpolation network are trained with the classifier in an end-to-end setup.

3 PROPOSED METHOD

Our paper focuses on the problem of time series classification of irregularly sampled and unaligned time series. We first define the required terms before describing our models

3.1 NOTATION & REQUIREMENTS

Definition 1 (Time series). *We describe a time series of an instance i as a set $\mathcal{S}_i$ of $M := \text{len}(\mathcal{S}_i)$ observations s_j such that $\mathcal{S}_i := \{s_1, \ldots, s_M\}$. We assume each observation s_j to be represented*
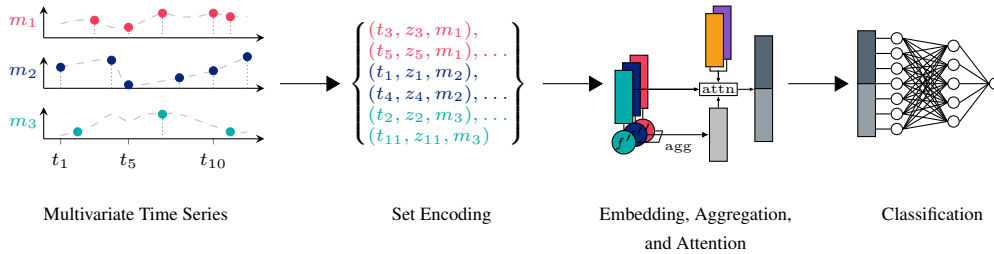
Figure 1: Schematic overview of SEFT's architecture. The first panel exemplifies a potential input, namely a multivariate time series, consisting of 3 modalities m_1, m_2, m_3. We treat the jth observation as a tuple (t_j, z_j, m_j), comprising a time t_j, a value z_j, and a modality indicator m_j. All observations are summarized as a set of such tuples. Each set of tuples belonging to the same modality is then separately embedded (f') and subsequently aggregated (`agg`). An attention mechanism (`attn`) as described in Section 3.3 is then applied to learn the importance of individual and consecutive observations. Respective query matrices for 2 attentions head are illustrated in purple and orange blocks. The results of each attention head are then concatenated and used as the input for final classification layers.

as a tuple (t_j, z_j, m_j), consisting of a time $t_j \in \mathbb{R}^+$, an observed value $z_j \in \mathbb{R}$, and a modality indicator $m_j \in \{1 \dots D\}$, where D represents the dimensionality of the time series. We write $\Omega \subseteq \mathbb{R}^+ \times \mathbb{R} \times \mathbb{N}^+$ to denote the domain of observations. An entire time series can thus be represented as

$$\mathcal{S}_i := \{(t_1, z_1, m_1), \dots, (t_M, z_M, m_M)\}, \tag{1}$$

where for notational convenience we omitted the index i.

We leave this definition very general on purpose, allowing the length of each time series (comprising all channels of one instance) to differ, since our models are capable of handling this. Likewise, we neither enforce nor expect all time series to be synchronized, i.e. being sampled at the same time, but rather we permit unaligned or *non-synchronized* observations in the sense of not having to observe all modalities at each time point. Time series are collected in a dataset $\mathcal{D}$.

Definition 2 (Dataset). *We consider a dataset $\mathcal{D}$ to contain n time series. Elements of $\mathcal{D}$ are tuples, i.e. $\mathcal{D} := \{(\mathcal{S}_1, y_1), \dots, (\mathcal{S}_N, y_N)\}$, where $\mathcal{S}_i$ denotes the ith time series and $y_i \in \{1, \dots, C\}$ its associated class label.*

Figure 1 gives a high-level overview of our method, including the individual steps required to perform classification. To get a more intuitive grasp of these definitions, we briefly illustrate our time series notation with an example. Let instance i be an in-hospital patient, while the time series represent measurements of two channels of vital parameters during a hospital stay, namely heart rate (HR) and mean arterial blood pressure (MAP). We enumerate those channels as modalities 1 and 2. Counting from admission time, a HR of 60 and 65 beats per minute was measured after 0.5 h and 3.0 h, respectively, whereas MAP values of 80, 85, and 87 mmHg were observed after 0.5 h, 1.7 h, and 2.5 h. According to Definition 1, the time series is thus represented as $\mathcal{S}_i = \{(0.5, 60, 1), (3, 65, 1), (0.5, 80, 2), (1.7, 85, 2), (3, 87, 2)\}$. In this example, observations are ordered by modality to increase readability; in practice, we are dealing with unordered sets.

Definition 3 (Non-synchronized time series). *We call a D-dimensional time series non-synchronized if there is at least one time point $t_j \in \mathbb{R}^+$ at which at least one modality is not observed, i.e. if there exists $t_j \in \mathbb{R}^+$ such that $|\{(t_k, z_k, m_k) \mid t_k = t_j\}| \neq D$.*

Furthermore, we assume that no two measurements of the same modality m_k occur at the same time, i.e. $t_i \neq t_j$ for $i \neq j$ has to be satisfied for all measurements in m_k. This assumption is not required for *technical* reasons but for *consistency*. It also makes it possible to interpret the results later on.

To summarize our generic setup, we do not require M, the number of observations per time series, to be the same, i.e. $\text{len}(\mathcal{S}_i) \neq \text{len}(\mathcal{S}_j)$ for $i \neq j$ is permitted, nor do we assume that the time points and modalities of the observations are the same across time series. This setting is common in biomedical

time series, for example. Since typical machine learning algorithms are designed to operate on data of a *fixed* dimension, novel approaches to this non-trivial problem are required.

3.2 OUR MODEL

In the following, we describe an approach inspired by differentiable learning of functions that operate on sets (Zaheer et al., 2017; Wagstaff et al., 2019). We phrase the problem of classifying time series on irregular grids as learning a function f on a set of arbitrarily many time series observations following Definition 1, i.e. $\mathcal{S} = \{(t_1, z_1, m_1), \ldots, (t_M, z_M, m_M)\}$, such that $f \colon \mathcal{S} \to \mathbb{R}^C$, where $\mathcal{S}$ represent a generic time series of arbitrary cardinality and $\mathbb{R}^C$ corresponds to the logits of the C classes in the dataset. As we previously discussed, we interpret each time series as an unordered set of measurements, where all information is conserved because the observation time is included for each set element. Following the framework of Zaheer et al. (2017), we define f to be a set function, i.e. a function that operates on a set and thus has to be *invariant* to the ordering of the elements in the set. We achieve these constraints by *sum-decomposing* f into the form

$$f(\mathcal{S}) = g\left(\frac{1}{|\mathcal{S}|} \sum_{s_j \in \mathcal{S}} h(s_j) \right) \tag{2}$$

where $h \colon \Omega \to \mathbb{R}^d$ and $g \colon \mathbb{R}^d \to \mathbb{R}^C$ are neural networks, $d \in \mathbb{N}^+$ determines the dimensionality of the latent representation, and s_j represents a single observation of the time series $\mathcal{S}$. We can view the averaged representations $1/|\mathcal{S}| \sum_{s_j \in \mathcal{S}} h(s_j)$ in general as a dataset-specific summary statistic learned to *best* distinguish the class labels. Equation 2 also implies the beneficial scalability properties of our approach: each embedding can be calculated independently of the others; hence, the constant computational cost of passing a single observation through the function h is scaled by the number of observations, resulting in a runtime of $\mathcal{O}(M)$ for a time series of length M.

Recently, Wagstaff et al. (2019) derived requirements for a practical universal function representation of *sum-decomposable* set functions, i.e the requirements *necessary* for a *sum-decomposable* function to represent an arbitrary set-function given that h and g are arbitrarily expressive. In particular, they show that a universal function representation can only be guaranteed provided that $d \geq \max_i \text{len}(\mathcal{S}_i)$ is satisfied. During hyperparameter search we thus independently sample the dimensionality of the aggregation space, and allow it to be in the order of the number of observations that are to be expected in the dataset. Further, we explored the utilization of max, sum, and mean as alternative aggregation functions inspired by Zaheer et al. (2017); Garnelo et al. (2018).

Intuition Our method can be connected to Takens's embedding theorem (Takens, 1981) for dynamical systems: we also observe a set of samples from some unknown (but deterministic) dynamical process; provided the dimensionality of our architecture is sufficiently large[1], we are capable of reconstructing the system up to diffeomorphism. The crucial difference is that we do *not* have to construct a time-delay embedding but rather, we let the network learn an embedding that is suitable for classification.

Time encoding In order to represent the time point of an observation on a normalized scale, we employ variant of *positional encodings*, as introduced by Vaswani et al. (2017). Preliminary results indicated that this encoding scheme reduces the sensitivity towards initialization and training hyperparameters of a model. Specifically, the time encoding converts the one-dimensional time axis into a multi-dimensional input by passing the time t of each observation through multiple sine and cosine functions of varying frequencies. Given a step size $\tau \in \mathbb{N}^+$, we refer to the encoded position as $x \in \mathbb{R}^\tau$, where

$$x_{2i}(t) := \sin\left(\frac{t}{\text{max\_ts}^{2i/\tau}} \right) \tag{3}$$

$$x_{2i+1}(t) := \cos\left(\frac{t}{\text{max\_ts}^{2i/\tau}} \right) \tag{4}$$

---

[1]In Takens's embedding theorem, $d > d_B$ is required, where d_B refers to the fractal box counting dimension (Liebovitch & Toth, 1989), which is typically well below the size of typical neural network architectures.

and max_ts represents the maximal time scale that is expected in the data. More precisely, we select the wavelengths using a geometric progression from 2π to max_ts $\cdot 2\pi$, and treat the number of steps and the maximal timescal max_ts as hyperparameters of the model. For all experiments time encodings were used, such that an observation is represented as $s_j = (x(t_j), z_j, m_j)$.

Loss function If not mentioned otherwise, we choose h and g in Equation 2 to be *multilayer perceptron* deep neural networks, parametrized by weights θ and ψ, respectively. We thus denote these neural networks by h_θ and g_ψ; their parameters are shared across all instances per dataset. In our training setup, we follow Zaheer et al. (2017) and apply the devised set function to the complete time series, i.e. to the set of all observations for each time series. Overall, we optimize a loss function that is defined as

$$\mathcal{L}(\theta, \psi) := \mathbb{E}_{(\mathcal{S}, y) \in \mathcal{D}} \left[\ell \left(y; g_\psi \left(\frac{1}{|\mathcal{S}|} \sum_{s_j \in \mathcal{S}} h_\theta(s_j) \right) \right) \right], \tag{5}$$

where $\ell(\cdot)$ represents a task-specific loss function.

3.3 ATTENTION-BASED AGGREGATION

So far, our method permits encoding sets of arbitrary sizes into a fixed-size representation. For increasingly large set sizes, however, many irrelevant observations could influence the result of the set function. The *mean* aggregation function is particularly susceptible to this because the influence of an observation to the embedding shrinks proportionally to the size of the set. We thus suggest to use a *weighted* mean in order to allow the model to decide which observations are relevant and which should be considered irrelevant. This is equivalent to computing an attention $a(\mathcal{S}, s_j)$ over the set input elements, and subsequently, computing the sum over all elements in the set.

Our approach is based on *scaled dot-product attention* with multiple heads m in order to be able to cover different aspects of the aggregated set. We define $a(\cdot)$ to depend on the overall set of elements, by computing an embedding of the set elements using a smaller set function f' and projecting the concatenation of the set representation and the individual set elements into the dot-product space of dimensionality d, i.e. $K_{j,i} = [f'(\mathcal{S}), s_j]^T W_i$ where $W_i \in \mathbb{R}^{\text{im}(f') + |s_j| \times d}$, $i \in \{1 \ldots m\}$, and $K \in \mathbb{R}^{|\mathcal{S}| \times d}$. Furthermore, we define a matrix of query points $Q \in \mathbb{R}^{m \times d}$, which allow the model to summarize different aspects of the dataset via

$$e_{j,i} = \frac{K_{j,i} \cdot Q_i}{\sqrt{m}} \qquad \text{and} \qquad a_{j,i} = \frac{\exp(e_{j,i})}{\sum_j \exp(e_{j,i})}$$

where $a_{j,i}$ represents the amount of attention that head i gives to set element j. For each head, we multiply the set element embeddings computed via the set function f with the attentions derived for the individual instances, i.e. $r_i = \sum_j a_{j,i} f(s_j)$. The computed representation is concatenated and passed to the aggregation network h_θ as in a regular set function, i.e. $r* = [r_1 \ldots r_m]$. In our setup, we initialize Q with zeros, such that at the beginning of training, the attention mechanism is equivalent to computing the unweighted mean over the set elements.

4 EXPERIMENTS

We executed all experiments and implementations in a unified code base, which we also make available[2] to the community. While some of the datasets used subsequently have access restrictions, anybody can gain access after satisfying the defined requirements. This ensures the reproducibility of our results. Please consult Appendix A.2 for further details.

4.1 DATASETS

In order to benchmark the proposed method we selected 4 datasets with irregularly-sampled and non-synchronized measurements.

---

[2]https://osf.io/2hg74/?view_only=8d45fdf237954948a02f1e2bf701cdf1

Healing MNIST The `H-MNIST` dataset was introduced by Krishnan et al. (2015) in order to simulate characteristics which typically occur in medical time series. In our setup, we use a variant of this dataset. Every instance of the dataset contains 10 frames, derived from a single instance of `MNIST` dataset, where the digit is rotated according to an angle uniformly sampled between $-90°$ to $90°$. Furthermore, 3 randomly-selected consecutive frames are augmented by a square artefact in the top left corner of the image in order to indicate seasonality in the time series. Finally, 60 % of the data points are randomly discarded in order to yield a final high-dimensional irregularly-sampled time series with non-synchronized measurements. Using these settings each instance has on average $3,136$ observations.

MIMIC-III Tasks MIMIC-III (Johnson et al., 2016) is a widely-used, freely-accessible dataset containing around $50,000$ distinct ICU stays. The median length of stay is 2.1 d and a wide range of physiological measurements (e.g. arterial blood pressure, respiration rate, heart rate) are recorded with a resolution of 1 h. Furthermore, laboratory test results, collected at irregular time intervals are available. Recently, Harutyunyan et al. (2019) defined a set of machine learning tasks, labels, and benchmarks using a subset of the MIMIC-III data set. We trained and evaluated our method and competing methods on the binary mortality prediction task (`M3-Mortality`) and on the multiclass problem of phenotype classification (`M3-Phenotyping`), while applying additional filtering described in Appendix A.1. The goal of the mortality prediction task is to predict whether a patient will die during his/her hospital stay using only data from the first 48 hours of the ICU stay. This data set contains around $21,000$ stays of which approximately 10 % result in death. The phenotype classification task consists of $40,000$ patients, each of which can suffer from a multitude of 25 acute care conditions.

Physionet Mortality Prediction Challenge The 2012 Physionet challenge data set (Goldberger et al., 2000), which we abbreviate `P-Mortality`, contains $12,000$ ICU stays each of which lasts at least 48 h. For each stay, a set of general descriptors (such as gender, age, height, weight) were collected at admission time. Depending on the course of the stay and patient status, up to 37 time series variables were measured (e.g. blood pressure, lactate, respiration rate, temperature). While some modalities might be measured in regular time intervals (e.g. hourly or daily), some are only collected when required. Not all variables are available for each stay. The goal of the challenge was to predict if—and with which certainty —a patient will die during the hospital stay. The training set consists of $8,000$ stays while the testing set comprises $4,000$ ICU visits. Both data sets are similarly imbalanced, with a prevalence of around 14 %. For simplicity, the general descriptors (such as age and weight), were included as time points with a single observation at the beginning of the stay. This treatment is similar to the approach by Harutyunyan et al. (2019) in the MIMIC-III benchmarking datasets. Please refer to Table 2, Table 3, and Table 4 in the appendix for a more detailed enumeration of samples sizes and label distributions. The total number of samples may slightly deviate from the originally published splits, as time series of excessive length prevented fitting some methods in reasonable time, and were therefore excluded.

4.2 COMPETITOR METHODS

GRU-simple GRU-SIMPLE (Che et al., 2018) augments the input at time t of a Gated-Recurrent-Unit RNN with a measurement mask m_t^d and a δ_t matrix, which contains the time since the last measurement of the corresponding modality d, such that

$$\delta_t = \begin{cases} s_t - s_{t-1} + \delta_{t-1}^d & t > 1, m_{t-1}^d = 0 \\ s_t - s_{t-1} & t > 1, m_{t-1}^d = 1 \\ 0 & t = 0 \end{cases}$$

where s_t represents the time associated with time step t.

Phased-LSTM The PHASED-LSTM (Neil et al., 2016) introduced a biologically inspired time dependent gating mechanism which regulates access to the hidden and cell state of a Long short-term RNN cell (Hochreiter & Schmidhuber, 1997). While this allows the network to handle event-based sequences with irregularly spaced observations, the approach does not support unaligned measurements. In order to still provide the architecture with all relevant information, we augment the input in a similar fashion as described for the GRU-SIMPLE approach.

GRU-D GRU-D or GRU-Decay (Che et al., 2018) contains modifications to the GRU RNN cell, allowing it to decay past observations to the mean imputation of a modality using a learnable decay

Table 1: Performance comparison of methods on benchmarking datasets. Performance metrics have been rescaled to 100 for readability reasons. "AUC" denotes the area under the Receiver Operating Characteristic (ROC) curve; "PR AUC" denotes the area under the precision recall curve.

DATASET	MODEL	MICRO AUC	MACRO AUC	WEIGHTED AUC	RUNTIME
H–MNIST	GRU-SIMPLE	99.09 ± 0.05	99.01 ± 0.05	99.03 ± 0.05	11.43 ± 0.47
	PHASED-LSTM	98.63 ± 0.13	98.50 ± 0.15	98.52 ± 0.14	33.93 ± 1.11
	GRU-D	99.42 ± 0.01	99.37 ± 0.02	99.38 ± 0.02	11.81 ± 0.44
	IP-NETS	99.06 ± 0.05	98.96 ± 0.03	98.98 ± 0.03	127.76 ± 0.95
	SEFT*	$\mathbf{99.76 \pm 0.01}$	$\mathbf{99.75 \pm 0.01}$	$\mathbf{99.75 \pm 0.01}$	$\mathbf{4.05 \pm 0.35}$
M3-Phenotyping	GRU-SIMPLE	79.89 ± 0.14	73.91 ± 0.19	72.55 ± 0.16	112.58 ± 2.03
	PHASED-LSTM	80.00 ± 0.06	73.91 ± 0.09	72.65 ± 0.08	400.41 ± 14.14
	GRU-D	$\mathbf{82.16 \pm 0.04}$	$\mathbf{77.14 \pm 0.03}$	$\mathbf{76.08 \pm 0.01}$	288.70 ± 16.66
	IP-NETS	-	-	-	-
	SEFT	81.22 ± 0.12	75.95 ± 0.09	74.90 ± 0.11	56.27 ± 2.14
	SEFT-ATTN	82.00 ± 0.06	76.95 ± 0.09	75.88 ± 0.09	$\mathbf{52.32 \pm 0.74}$
		ACCURACY	PR AUC	AUC	RUNTIME
M3-Mortality	GRU-SIMPLE	88.24 ± 0.38	36.36 ± 1.31	79.36 ± 0.26	22.80 ± 0.56
	PHASED-LSTM	88.32 ± 0.31	35.30 ± 1.38	80.16 ± 0.22	25.54 ± 0.26
	GRU-D	$\mathbf{89.56 \pm 0.38}$	$\mathbf{46.76 \pm 0.65}$	83.73 ± 0.21	31.85 ± 0.86
	IP-NETS	89.73 ± 0.16	45.88 ± 0.87	83.30 ± 0.56	101.12 ± 4.52
	SEFT	88.65 ± 0.49	36.18 ± 5.07	79.15 ± 3.00	$\mathbf{3.72 \pm 0.11}$
	SEFT-ATTN	89.48 ± 0.16	45.25 ± 0.96	$\mathbf{83.79 \pm 0.59}$	16.64 ± 0.20
P-Mortality	GRU-SIMPLE	85.66 ± 0.14	39.43 ± 0.71	79.79 ± 0.16	5.16 ± 0.06
	PHASED-LSTM	85.57 ± 0.11	39.55 ± 0.62	78.71 ± 0.76	18.59 ± 1.15
	GRU-D	87.19 ± 0.30	$\mathbf{54.95 \pm 0.54}$	$\mathbf{86.58 \pm 0.32}$	14.08 ± 0.38
	IP-NETS	87.23 ± 0.18	54.87 ± 0.41	86.42 ± 0.18	7.21 ± 0.46
	SEFT	87.11 ± 0.32	52.07 ± 0.41	84.12 ± 0.32	$\mathbf{3.07 \pm 0.03}$
	SEFT-ATTN	$\mathbf{87.62 \pm 0.16}$	54.05 ± 0.27	85.50 ± 0.13	7.54 ± 0.08

*: Due to the high dimensionality of HealingMNIST and associated memory issues, the set elements were constructed by simply combining the observation time with all values and measurement indicators.

rate. By additionally providing the measurement masks as an input the recurrent neural network the last feed in value. Learns how fast to decay back to a mean imputation of the missing data modality.

Interpolation Prediction Networks IP-NETWORKS (Shukla & Marlin, 2019) apply multiple semi-parametric interpolation schemes to irregularly-sampled time series to obtain regularly-sampled representations that cover long-term trends, transients, and also sampling information. The method combines a univariate interpolation step with a subsequent multivariate interpolation; the parameters of the interpolation network are trained with the classifier in an end-to-end fashion.

4.3 RESULTS

To permit a fair comparison between the methods, we executed hyperparameter searches for each model on each dataset, composed of uniformly sampling 20 parameters according to Appendix A.3. Training was stopped after 20 epochs without improvement of the validation loss, the hyperparameters with the best overall validation performance were selected for quantifying the performance on the test set. The train, validation, and test splits were the same for all models and all evaluations. Final performance on the test set was calculated by 3 *independent* runs of the models; evaluation took place after the model was restored to the state with the best validation loss. The results are shown in Table 1. Overall, our proposed method exhibits the *lowest* per-epoch runtime on all datasets, while either yielding competitive or state-the-art performance on medical time series datasets.

Opening the black box   In the medical domain, it is of particular interest to understand the decisions a model makes based on the input it is provided with. The formulation of our model and its *per observation* perspective on time series gives it the unique property of being able to quantify to which extent an individual observation contributed to the output of the model. We exemplify this in
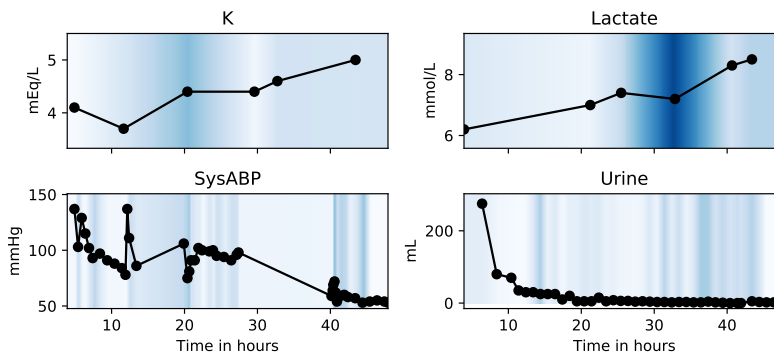
Figure 2: Visualizations of a single attention head on an instance of the `P-Mortality` dataset. We display a set of variables relevant for assessing patient stability and organ failure: Serum Potassium (K), Lactate, Systolic Arterial Blood Pressure (SysABP), and Urine output. Darker colors represent higher attention values.

Figure 2 with a patient time series that was combined with our models attention values, displayed for a set of clinically relevant variables. After reviewing these records with our medical expert, we find that our model is able to pick up regions with drastic changes in individual modalities. Moreover, it is able to inspect other modalities at the same associated time (for instance, at hour 20). This is behaviour similar to what one would expect from an alerted clinician reviewing the logged medical records. Interestingly, we observe that the model attends to *known* trends (that are consisting with domain knowledge about patient deterioration ultimately resulting in death) such as increase in lactate or hemodynamic instability, as indicated by drops in blood pressure. Furthermore, the model appears to be alerted by persisting low urine output. After several hours, this can be indicative of kidney failure.

5 CONCLUSION

In this work, we presented a novel approach for classifying time series with irregularly-sampled and unaligned, that is *non-synchronized*, observations. Our approach yields state-of-the-art to strongly competitive performance on numerous simulated and real-world datasets, while reducing runtime by almost half. Moreover, we demonstrated that combining the perspective of individual observations with an attention mechanism permits increasing the interpretability of the model. This is particularly relevant for the medical and healthcare applications.

For future work, we reserve a more extensive exploration of the learned latent representation to evaluate its utility for clustering of time series or visualization of their similarity.

REFERENCES

Edwin V. Bonilla, Kian M Chai, and Christopher Williams. Multi-task gaussian process prediction. In *Advances in Neural Information Processing Systems (NeurIPS)*, pp. 153–160, 2008.

Zhengping Che, Sanjay Purushotham, Kyunghyun Cho, David Sontag, and Yan Liu. Recurrent neural networks for multivariate time series with missing values. *Scientific reports*, 8(1):6085, 2018.

Joseph Futoma, Sanjay Hariharan, and Katherine Heller. Learning to detect sepsis with a Multitask Gaussian Process RNN classifier. In *International Conference on Machine Learning (ICML)*, pp. 1174–1182, 2017.

Marta Garnelo, Dan Rosenbaum, Christopher Maddison, Tiago Ramalho, David Saxton, Murray Shanahan, Yee Whye Teh, Danilo Rezende, and SM Ali Eslami. Conditional neural processes. In *International Conference on Machine Learning*, pp. 1690–1699, 2018.

Ary L. Goldberger, Luis A.N. Amaral, Leon Glass, Jeffrey M. Hausdorff, Plamen Ivanov, Roger G. Mark, Joseph E. Mietus, George B. Moody, Chung-Kang Peng, and H. Eugene Stanley. Physiobank, physiotoolkit, and physionet: components of a new research resource for complex physiologic signals. *Circulation*, 101(23):e215–e220, 2000.

Hrayr Harutyunyan, Hrant Khachatrian, David C. Kale, Greg Ver Steeg, and Aram Galstyan. Multitask learning and benchmarking with clinical time series data. *Scientific Data*, 6(1):96, 2019. ISSN 2052-4463.

Sepp Hochreiter and Jürgen Schmidhuber. Long short-term memory. *Neural Computation*, 9(8): 1735–1780, 1997.

Alistair E. W. Johnson, Tom J. Pollard, Lu Shen, Li-wei H. Lehman, Mengling Feng, Mohammad Ghassemi, Benjamin Moody, Peter Szolovits, Leo Anthony Celi, and Roger G. Mark. MIMIC-III, a freely accessible critical care database. *Scientific Data*, 3, 2016.

Rahul G. Krishnan, Uri Shalit, and David Sontag. Deep Kalman Filters. *arXiv e-prints*, art. arXiv:1511.05121, Nov 2015.

Steven Cheng-Xian Li and Benjamin M Marlin. Classification of sparse and irregularly sampled time series with mixtures of expected gaussian kernels and random features. In *UAI*, pp. 484–493, 2015.

Steven Cheng-Xian Li and Benjamin M Marlin. A scalable end-to-end gaussian process adapter for irregularly sampled time series classification. In *Advances In Neural Information Processing Systems*, pp. 1804–1812, 2016.

Larry S. Liebovitch and Tibor Toth. A fast algorithm to determine fractal dimensions by box counting. *Physics Letters A*, 141(8):386–390, 1989.

Zachary C Lipton, David Kale, and Randall Wetzel. Directly modeling missing data in sequences with rnns: Improved classification of clinical time series. In *Machine Learning for Healthcare Conference*, pp. 253–270, 2016.

Roderick JA Little and Donald B Rubin. *Statistical analysis with missing data*, volume 333. John Wiley & Sons, 2014.

Zhengdong Lu, Todd K Leen, Yonghong Huang, and Deniz Erdogmus. A reproducing kernel hilbert space framework for pairwise time series distances. In *Proceedings of the 25th International Conference on Machine learning*, pp. 624–631, 2008.

Benjamin M Marlin, David C Kale, Robinder G Khemani, and Randall C Wetzel. Unsupervised pattern discovery in electronic health care data using probabilistic clustering models. In *Proceedings of the 2nd ACM SIGHIT International Health Informatics Symposium*, pp. 389–398. ACM, 2012.

Daniel Neil, Michael Pfeiffer, and Shih-Chii Liu. Phased lstm: Accelerating recurrent network training for long or event-based sequences. In *Advances in Neural Information Processing Systems (NeurIPS)*, pp. 3882–3890, 2016.

Satya Narayan Shukla and Benjamin Marlin. Interpolation-prediction networks for irregularly sampled time series. In *International Conference on Learning Representations*, 2019.

Floris Takens. Detecting strange attractors in turbulence. In David Rand and Lai-Sang Young (eds.), *Dynamical Systems and Turbulence*, pp. 366–381, Heidelberg, Germany, 1981. Springer.

Ashish Vaswani, Noam Shazeer, Niki Parmar, Jakob Uszkoreit, Llion Jones, Aidan N Gomez, Łukasz Kaiser, and Illia Polosukhin. Attention is all you need. In *Advances in Neural Information Processing Systems (NeurIPS)*, pp. 5998–6008, 2017.

Oriol Vinyals, Samy Bengio, and Manjunath Kudlur. Order matters: Sequence to sequence for sets. *arXiv preprint arXiv:1511.06391*, 2015.

Edward Wagstaff, Fabian B. Fuchs, Martin Engelcke, Ingmar Posner, and Michael Osborne. On the Limitations of Representing Functions on Sets. 2019.

Christopher K. Williams and Carl Edward Rasmussen. Gaussian processes for machine learning. *MIT Press*, 2(3):4, 2006.

Pranjul Yadav, Michael Steinbach, Vipin Kumar, and Gyorgy Simon. Mining electronic health records (EHRs): a survey. *ACM Computing Surveys*, 50(6):85, 2018.

Manzil Zaheer, Satwik Kottur, Siamak Ravanbakhsh, Barnabas Poczos, Ruslan R. Salakhutdinov, and Alexander J. Smola. Deep sets. In *Advances in Neural Information Processing Systems (NeurIPS)*, pp. 3391–3401, 2017.

A   Appendix

Table 2: `M3-Mortality` prevalence of labels for the binary classification task

	Training Prevalence	Testing Prevalence
In-hospital deaths	0.135	0.116

Table 3: `P-Mortality` prevalence of labels for the binary classification task

	Training Prevalence	Testing Prevalence
In-hospital deaths	0.140	0.146

A.1   Data filtering

Due to memory requirements of some of the competitor methods, it was necassary to excluded time series with extremely high number of measurements. For the `M3-Phenotyping` patients with more than 2000 distinct time points were discarded from training. For `M3-Mortality` patients with more than 1000 time points were discarded as they contained dramatically different measuring frequencies compared to the rest of the dataset.

A.2   Implementational details

All experiments were run using `tensorflow 0.15.0rc0` and training was performed on `NVIDIA Geforce GTX 1080` GPUs. In order to allow a fair comparison between methods, the input processing pipeline cached model specific representations and transformations of the data. To further increase efficiency of the RNNs, sequences were binned in to buckets of jointly trained instances depending on their sequence length. The buckets were determined according to the $(0.25, 0.5, 0.75)$ quantiles of the length distributions of the datasets.

A.3   Training and hyperparameter search

General   All models were trained using the Adam optimizer, while randomly sampling the learning rate from $(0.001, 0.0005, 0.00025, 0.0001)$. Further, the batch size of all methods was sampled from the values $(32, 64, 128, 256)$.

Recurrent neural networks   For the RNN based methods (GRU-Simple, Phased-LSTM, GRU-D and IP-Nets), the number of units was sampled in from the values $(16, 32, 64, 128, 256, 512)$. Further, recurrent dropout and input dropout were sampled from the values $(0.0, 0.1, 0.2, 0.3)$. Solely, for the Phased-LSTM method, we did not apply dropout to the recurrent state and the inputs, as the learnt frequencies were hypothesized to fulfill a similar function as dropout (Neil et al., 2016).

SeFT   We vary the number of layers, dropout in between the layers and the number of nodes per layer for both the encoding network h_θ and the aggregation network g_ψ from the same ranges. The number of layers is randomly sampled between 1 and 5, the number of nodes in a layer are uniformly sampled from the range $(16, 32, 64, 128, 256, 512)$ and the dropout fraction is sampled from the values $(0.0, 0.1, 0.2, 0.3)$. The width of the embedding space prior to aggregation is sampled from the values $(32, 64, 128, 256, 512, 1024, 2048)$. The aggregation function selected to be one of $mean$, sum and max. The number of dimensions used for the positional embedding τ is selected uniformly from $(4, 8, 16)$ and max_ts us selected from the values $(10, 100, 1000)$.

SeFT-Attn   The parameters for the encoding and aggregation networks are sampled in a similar fashion as for SeFT. In contrast we set the aggregation function to be sum as described in the text.

Table 4: `M3-Phenotyping` prevalence of labels for the multi label classification task

Phenotype	Training Prevalence	Validation Prevalence	Testing Prevalence
Acute and unspecified renal failure	0.216	0.207	0.211
Acute cerebrovascular disease	0.0746	0.0753	0.0662
Acute myocardial infarction	0.103	0.103	0.108
Cardiac dysrhythmias	0.322	0.317	0.323
Chronic kidney disease	0.135	0.131	0.132
Chronic obstructive pulmonary disease and bronchiectasis	0.132	0.128	0.126
Complications of surgical procedures or medical care	0.207	0.201	0.213
Conduction disorders	0.0726	0.07	0.0704
Congestive heart failure; nonhypertensive	0.268	0.264	0.268
Coronary atherosclerosis and other heart disease	0.323	0.317	0.331
Diabetes mellitus with complications	0.0955	0.0945	0.094
Diabetes mellitus without complication	0.194	0.187	0.192
Disorders of lipid metabolism	0.291	0.287	0.289
Essential hypertension	0.421	0.41	0.424
Fluid and electrolyte disorders	0.267	0.276	0.265
Gastrointestinal hemorrhage	0.0715	0.0747	0.0788
Hypertension with complications and secondary hypertension	0.133	0.131	0.13
Other liver diseases	0.0884	0.0904	0.0883
Other lower respiratory disease	0.0514	0.0484	0.0565
Other upper respiratory disease	0.0408	0.0371	0.0429
Pleurisy; pneumothorax; pulmonary collapse	0.0858	0.09	0.0905
Pneumonia (except that caused by tuberculosis or sexually transmitted disease)	0.14	0.135	0.135
Respiratory failure; insufficiency; arrest (adult)	0.18	0.184	0.177
Septicemia (except in labor)	0.142	0.145	0.138
Shock	0.0783	0.0745	0.0811
Total samples	29 208	6359	6266

Further we use a constant architecture for the attention network f' with 2 layers, 64 nodes per layer, 4 heads and a dimensionality of the dot product space d of 128. We solely sample the amount of attention dropout uniformly from the values $(0.0, 0.1, 0.25, 0.5)$.